

Determining the WIMP mass using direct detection experiments

Anne M. Green[†]

[†] School of Physics and Astronomy, University of Nottingham, University Park, Nottingham, NG7 2RD, UK

E-mail: anne.green@nottingham.ac.uk

Abstract.

We study the accuracy with which the WIMP mass could be determined by a superCDMS-like direct detection experiment, given optimistic assumptions about the detector set-up and WIMP properties. We consider WIMPs with an interaction cross-section of $\sigma_p = 10^{-7}$ pb (just below current exclusion limits) and assume, initially, that the local WIMP velocity distribution and density are known and that the experiment has negligible background. For light WIMPs (mass significantly less than that of the target nuclei) small variations in the WIMP mass lead to significant changes in the energy spectrum. Conversely for heavy WIMPs the energy spectrum depends only weakly on the WIMP mass. Consequently it will be far easier to measure the WIMP mass if it is light than if it is heavy. With exposures of $\mathcal{E} = 3 \times 10^3$, 3×10^4 and 3×10^5 kg day (corresponding, roughly, to the three proposed phases of SuperCDMS) it will be possible, given the optimistic assumptions mentioned above, to measure the mass of a light WIMP with an accuracy of roughly 25%, 15% and 2.5% respectively. These numbers increase with increasing WIMP mass, and for heavy WIMPs, $m_\chi > \mathcal{O}(500 \text{ GeV})$, even with a large exposure it will only be possible to place a lower limit on the mass. Finally we discuss the validity of the various assumptions made, and the consequences if these assumptions are not valid. In particular if the local WIMP distribution is composed of a number of discrete streams it will not be possible to determine the WIMP mass.

Keywords: dark matter, dark matter detectors

1. Introduction

Diverse cosmological observations indicate that the majority of the matter in the Universe is dark and non-baryonic (e.g. Ref. [1]). Weakly Interacting Massive Particles (WIMPs) are one of the leading cold dark matter candidates, and supersymmetry provides a concrete, well-motivated, WIMP candidate in the form of the lightest neutralino (e.g. Ref. [2, 3]). The direct detection of WIMPs in the lab [4] would not only directly confirm the existence of dark matter but would also probe the parameters of supersymmetry models. Constraints on, or measurements of, the WIMP mass and interaction cross-section will be complementary to the information derived from collider experiments [5, 6]. It is therefore pertinent to examine the accuracy with which WIMP direct detection experiments will be able to measure the WIMP mass, if they detect WIMPs.

Direct detection experiments could potentially measure the WIMP mass via the mass dependence of either the energy spectrum [7] or the ‘crossing energy’ at which the phase of the annual modulation signal [8], due to the motion of the Earth, changes sign [9, 10, 11]. The size of the annual modulation signal is small (of order a few per cent), however, and given the current exclusion limits from CDMS [12, 13] it is unlikely that even planned tonne scale experiments, such as SuperCDMS [14, 15], Xenon [16] and EURECA [17], will be able to accurately measure the energy dependence of the annual modulation phase [10, 18] ‡. Furthermore the shape, phase and amplitude of the annual modulation signal depend sensitively on the detailed local WIMP velocity distribution [22] whereas the shape of the differential event rate does not [23, 24], if the local WIMP distribution is smooth. The mass dependence of the differential event rate [7] (see also [25]) therefore appears to offer the best prospect, in the short to medium term at least, for probing the WIMP mass using direct detection experiments.

In this paper we examine the accuracy with which a future SuperCDMS [14, 15] like direct detection experiment will be able to measure the WIMP mass, given a positive detection. We consider the effect of varying the underlying WIMP mass and detector exposure, and also examine the uncertainties which arise from our lack of knowledge of the underlying WIMP distribution. In Sec. 2 we outline the calculation of the differential event rate and its dependence on the WIMP mass. We describe our Monte Carlo simulations and results in Sec. 3, discuss the validity of the assumptions made in Sec. 4 and conclude with discussion in Sec. 5.

‡ The DAMA collaboration have, with a NaI detector and an exposure of $\sim 1.1 \times 10^5$ kg day, observed an annual modulation, which they interpret as a WIMP signal [19], however it appears to be possible to reconcile this with the CDMS exclusion limit only by invoking ‘non-standard’ WIMP properties (such as the WIMP-proton and WIMP-neutron couplings being different [20] or WIMPs which can scatter inelastically [21]).

2. Differential event rate

2.1. Basic calculation

The direct detection differential event rate, or energy spectrum, depends on the WIMP mass, its interaction with the detector nuclei and the velocity distribution of the incoming WIMPs. Assuming purely spin-independent coupling, the event rate per unit energy, is given by (see e.g. [2, 7]):

$$\frac{dR}{dE}(E) = \frac{\sigma_p \rho_\chi}{2\mu_{p\chi}^2 m_\chi} A^2 F^2(E) \mathcal{F}(E), \quad (1)$$

where ρ_χ is the local WIMP density, σ_p the WIMP scattering cross section on the proton, $\mu_{p\chi} = (m_p m_\chi)/(m_p + m_\chi)$ the WIMP-proton reduced mass, A and $F(E)$ the mass number and form factor of the target nuclei respectively and E is the recoil energy of the detector nucleus. The dependence on the WIMP velocity distribution is encoded in $\mathcal{F}(E)$, which is defined as

$$\mathcal{F}(E) = \left\langle \int_{v_{\min}}^{\infty} \frac{f^E(v, t)}{v} dv \right\rangle, \quad (2)$$

where $f^E(v, t)$ is the (time dependent) WIMP speed distribution in the rest frame of the detector, normalized to unity and $\langle \dots \rangle$ denotes time averaging. This is calculated from the velocity distribution in the rest frame of the Galaxy, $f^G(\mathbf{v})$, via Galilean transformation: $\mathbf{v} \rightarrow \tilde{\mathbf{v}} = \mathbf{v} + \mathbf{v}^E(t)$ where $\mathbf{v}^E(t)$ is the Earth's velocity with respect to the Galactic rest frame. The lower limit of the integral, v_{\min} , is the minimum WIMP speed that can cause a recoil of energy E :

$$v_{\min} = \left(\frac{Em_A}{2\mu_{A\chi}^2} \right)^{1/2}, \quad (3)$$

where m_A is the atomic mass of the detector nuclei and $\mu_{A\chi}$ the WIMP-nucleon reduced mass. We use the Helm form factor [26] with parameter values as advocated by Lewin and Smith [7]. For most calculations we use the ‘standard halo model’, an isotropic isothermal sphere, for which the local WIMP velocity distribution, in the Galactic rest frame, is Maxwellian (c.f. Ref. [8])

$$f^G(\mathbf{v}) = N \left[\exp(-|\mathbf{v}|^2/v_c^2) - \exp(-v_{\text{esc}}^2/v_c^2) \right] \quad |\mathbf{v}| < v_{\text{esc}}, \quad (4)$$

$$f^G(\mathbf{v}) = 0 \quad |\mathbf{v}| > v_{\text{esc}}, \quad (5)$$

where N is a normalization factor, $v_c = 220 \text{ km s}^{-1}$ [27] and $v_{\text{esc}} = 540 \text{ km s}^{-1}$ [28] are the local circular and escape speeds respectively and we use the usual fiducial value for the local WIMP density, $\rho_\chi = 0.3 \text{ GeV cm}^{-3}$. We use the expressions for the time dependence of the Earth's velocity with respect to the Galactic rest frame from Ref. [7], to transform the velocity distribution into the lab frame.

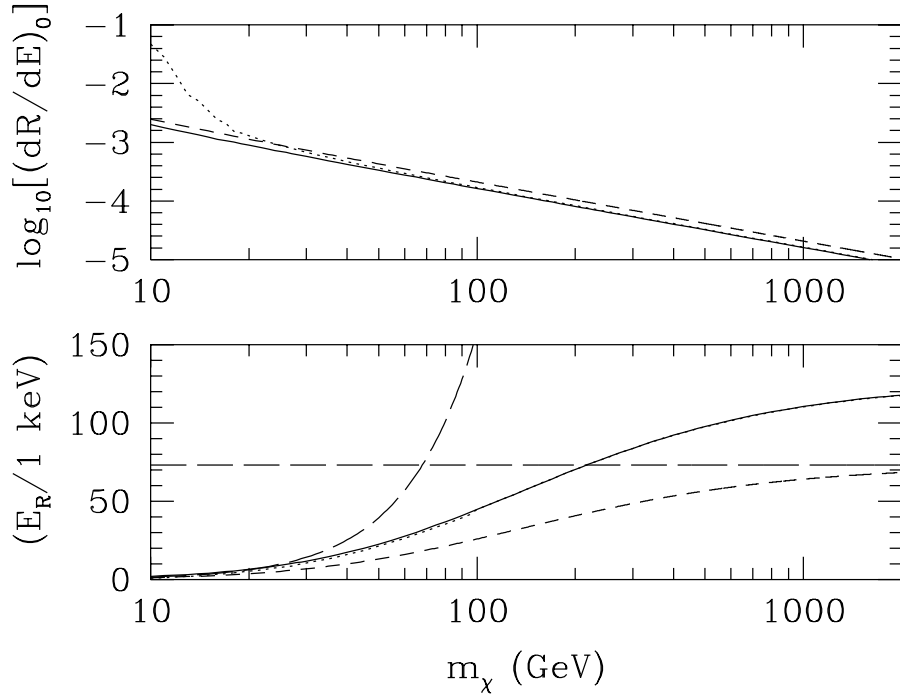


Figure 1. The differential event rate in the $E \rightarrow 0$ keV limit, $(dR/dE)_0$, (top panel) and the characteristic energy scale, E_R , (bottom panel) as a function of the WIMP mass, m_χ for a Ge detector. The solid (dotted) lines are the fits to the full calculation including the Earth’s velocity and the Galactic escape speed for threshold energy $E_{\text{th}} = 0$ (10) keV. The short dashed lines are eqs. (7) and (8) which neglect the Earth’s velocity and the Galactic escape speed. In the bottom panel the long dashed lines are the asymptotic mass dependences of E_R in the $m_\chi \ll m_A$ and $\gg m_A$ limits ($E_R \propto m_\chi^2$ and $\propto \text{const}$ respectively).

2.2. Dependence on the WIMP mass

The WIMP mass dependence of the differential event rate can most easily be seen, following Lewin and Smith [7], by first neglecting the Earth’s velocity and the Galactic escape speed. In this case eq. (1) can be written as

$$\frac{dR}{dE}(E) = \left(\frac{dR}{dE}\right)_0 \exp\left(-\frac{E}{E_R}\right) F^2(E), \quad (6)$$

where $(dR/dE)_0$, the event rate in the $E \rightarrow 0$ keV limit, and E_R , the characteristic energy scale, are given by

$$\left(\frac{dR}{dE}\right)_0 = \frac{\sigma_p \rho_\chi}{\sqrt{\pi} \mu_{p\chi}^2 m_\chi v_c} A^2, \quad (7)$$

and

$$E_R = \frac{2\mu_{A\chi}^2 v_c^2}{m_A}, \quad (8)$$

respectively. When the Earth’s velocity and the Galactic escape speed are taken into account eq. (1) is still a reasonable approximation to the event rate, provided that

multiplicative constants c_0 and c_{E_R} , are included in the expressions for $(\frac{dR}{dE})_0$ and E_R [7]. The exact values of the constants, which are of order unity, depend on the target nuclei, the energy threshold and the Galactic escape speed. We find, using least squares fitting to the full numerically calculated time averaged differential event for a Ge detector with energy threshold $E_{\text{th}} = 0 \text{ keV}$, $c_0 \approx 0.78$ and $c_{E_R} \approx 1.72$, with a weak dependence (in the 3rd significant figure) on the WIMP mass.

The mass dependence of $(dR/dE)_0$ and E_R for a Ge detector are shown in fig. 1. As expected from eq. (7), $(dR/dE)_0 \propto m_\chi^{-1}$, since $m_\chi \gg m_p$. Similarly as expected from eq. (8), for $m_\chi < m_A$, $E_R \propto m_\chi^2$. This mass dependence weakens with increasing WIMP mass, and E_R tends to its constant large mass asymptote for $m_\chi \sim \mathcal{O}(1 \text{ TeV})$. We will see below that this has important consequences for the determination of the WIMP mass from direct detection experiments. If, anticipating section III, we only fit to the event rate above an energy threshold $E_{\text{th}} = 10 \text{ keV}$ we find that for WIMP masses below $\sim 100 \text{ GeV}$ the fitting constants depend on the WIMP mass (this is visible in fig. 1 as the deviation of the dotted lines from the solid lines for small WIMP masses). This illustrates that while eq. 6 is a useful approximation for demonstrating the mass dependence of the energy spectrum, for concrete applications the time average of the local WIMP velocity distribution should be calculated explicitly.

3. Monte Carlo simulations

We use Monte Carlo simulations to examine, for a range of detector exposures and input WIMP masses, how well the WIMP mass could be determined from the energies of observed WIMP nuclear recoil events.

3.1. Detector properties

Our simulated detector is based on the proposed SuperCDMS experiment [14, 15], being composed of Ge with a nuclear recoil energy threshold $E_{\text{th}} = 10 \text{ keV}$. We assume that the background event rate is negligible, as is expected for this experiment located at SNOLab [14, 15], and that the energy resolution is perfect. For simplicity we assume that the nuclear recoil detection efficiency is independent of energy. The energy dependence of the efficiency of the current CDMS experiment is relatively small (it increases from ~ 0.46 at $E = 20 \text{ keV}$, the energy above which data from all detectors is analyzed, to ~ 0.51 at 100 keV [13]). For further discussion of these assumptions see Sec. 4.

The proposed SuperCDMS detector consists of 3 phases, with detector masses of $\sim 25 \text{ kg}$, 150 kg and 1 ton . We consider efficiency weighted exposures $\S \mathcal{E} = 3 \times 10^2, 3 \times 10^3, 3 \times 10^4$ and $3 \times 10^5 \text{ kg day}$. The later three exposures correspond, roughly, to a detector with mass equal to that of the 3 proposed phases of SuperCDMS taking data for a year || with a $\sim 50\%$ detection efficiency.

\S For brevity we subsequently refer to this as simply the exposure.

|| Accumulating this much ‘live-time’ would of course take substantially longer than a year.

3.2. WIMP properties

We assume a fixed WIMP-nucleon cross-section of $\sigma_p = 10^{-7}$ pb, which is just below the current exclusion limit from the CDMS experiment [12]. Since the number of events expected in a given experimental set-up is directly proportional to the cross-section, there is a straight-forward scaling to other cross-sections i.e. an exposure $\mathcal{E} = 3 \times 10^4$ kg day for $\sigma_p = 10^{-7}$ pb is equivalent to an exposure of $\mathcal{E} = 3 \times 10^5$ kg day for $\sigma_p = 10^{-8}$ pb. We consider input WIMP masses of $m_\chi = 25, 50, 100, 250$ and 500 GeV, with a Maxwellian speed distribution with circular speed $v_c = 220$ km s $^{-1}$. For $m_\chi = 100$ GeV we also consider circular speeds in the range $v_c = 180$ to 260 km s $^{-1}$ [27] and variations in the form of the speed distribution.

3.3. Statistical analysis

We estimate the WIMP mass and cross-section by maximizing the extended maximum function (which takes into account the fact that the number of events observed in a given experiment is not fixed) e.g. Ref. [29]:

$$L = \frac{\lambda^{N_{\text{expt}}} \exp(-\lambda)}{N_{\text{expt}}!} \prod_{i=1}^{N_{\text{expt}}} f(E_i). \quad (9)$$

Here N_{expt} is the number of events observed, E_i ($i = 1, \dots, N_{\text{expt}}$) are the energies of the events observed, $f(E)$ is the, normalized, differential event rate and $\lambda = \mathcal{E} \int_{E_{\text{th}}}^{\infty} (dR/dE) dE$ is the mean number of events ($f(E)$ and λ depend on m_χ and σ_p). We calculate the probability distribution of the maximum likelihood estimators, for each exposure and input WIMP mass, by simulating 10^4 experiments. We first calculate the expected number of events, $\lambda_{\text{in}} = \mathcal{E} \int_{E_{\text{th}}}^{\infty} (dR/dE) dE$, from the input energy spectrum. The actual number of events for a given experiment, N_{expt} , is drawn from a Poisson distribution with mean λ_{in} . We Monte Carlo generate N_{expt} events from the input energy spectrum, from which the maximum likelihood (hereafter ‘ML’) mass and cross-section are calculated.

Finally we plot the distribution of ML masses and cross sections. Given real data from a single experiment a Bayesian analysis with priors on the WIMP parameters, possibly based on the results of other experiments, would be a reasonable approach. However, the question which we are trying to address (‘For a given underlying WIMP mass, how well can the mass be measured?’) is best answered by simply considering the distribution of ML masses and cross-sections. Since the approximations we make regarding the detector set-up and WIMP distribution and cross-section are optimistic, a real experiment would make less accurate determinations of the WIMP properties.

3.4. Results

In fig. 2 we plot the probability distribution of ML WIMP masses and cross-sections for input WIMP parameters $m_\chi = 100$ GeV and $\sigma_p = 10^{-7}$ pb. In this case both the input energy spectrum and the maximum likelihood analysis of the simulated events are

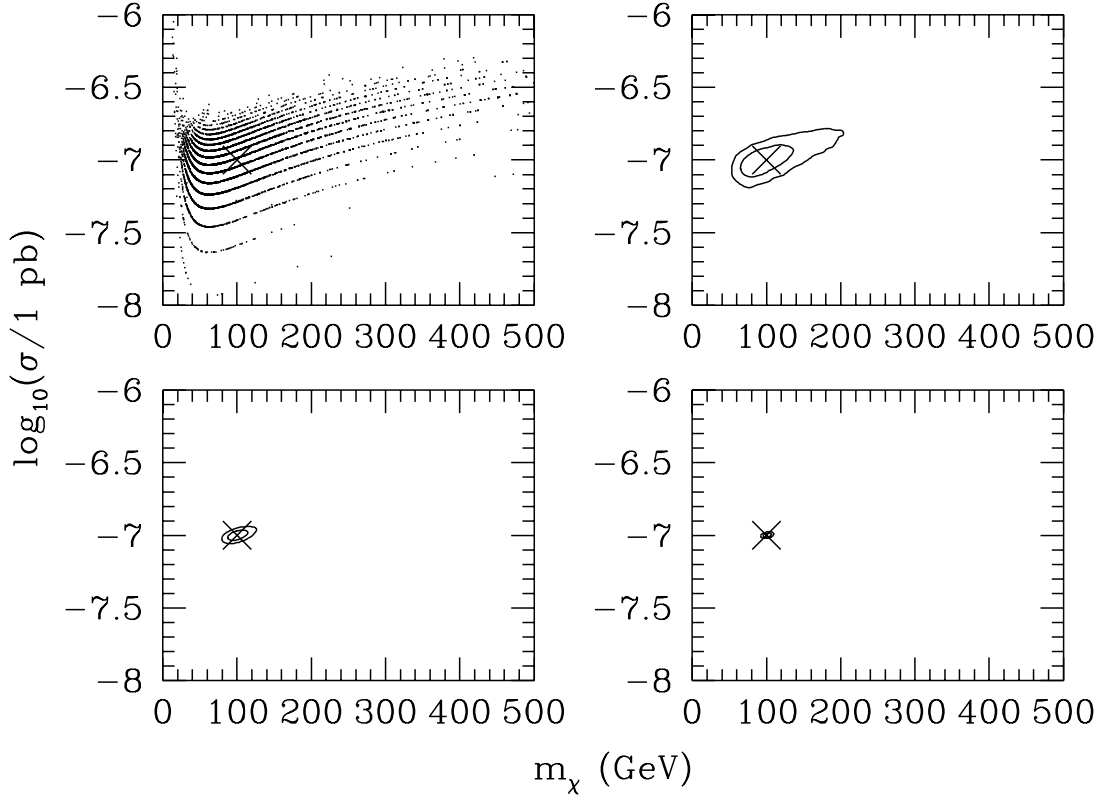


Figure 2. The distribution of the maximum likelihood WIMP masses, m_χ , and cross-sections, σ_p , for exposures of (top row, left to right and then bottom row left to right) $\mathcal{E} = 3 \times 10^2$, 3×10^3 , 3×10^4 and 3×10^5 kg day. For $\mathcal{E} = 3 \times 10^2$ kg day we explicitly plot the results from all 10^4 Monte Carlo experiments. For the larger exposures we plot contours containing 68% and 95% of the probability distribution. In each panel the large cross denotes the input parameters: $m_\chi = 100$ GeV, $\sigma_p = 10^{-7}$ pb.

carried out assuming a Maxwellian speed distribution with $v_c = 220 \text{ km s}^{-1}$. For each experiment the extended likelihood is maximized for WIMP parameters which produce an expected number of events equal to the actual number of events observed in that experiment: $\lambda(m_\chi, \sigma_p) = N_{\text{expt}}$. This means that, for fixed exposure, the ML parameters are localized on curves corresponding to fixed N_{expt} . For a given experiment the position of the ML parameters on the curve depends on the energies of the observed events. For $\mathcal{E} = 3 \times 10^2$ kg day, $\lambda_{\text{in}} = 7.8$, which is sufficiently small that the stratification of ML parameters is clearly visible and we hence plot the actual pairs of $m_\chi - \sigma_p$ values. For the larger exposures the mean number of events expected is proportionately larger, the stratification is no longer visible, the ML values are better localized in the $m_\chi - \sigma_p$ plane and we instead plot contours containing 68% and 95% of the simulated experiments. We calculate the continuous probability distribution of m_χ and σ_p by smoothing the ML values from the 10^4 Monte Carlo simulations with a double gaussian kernel and summing

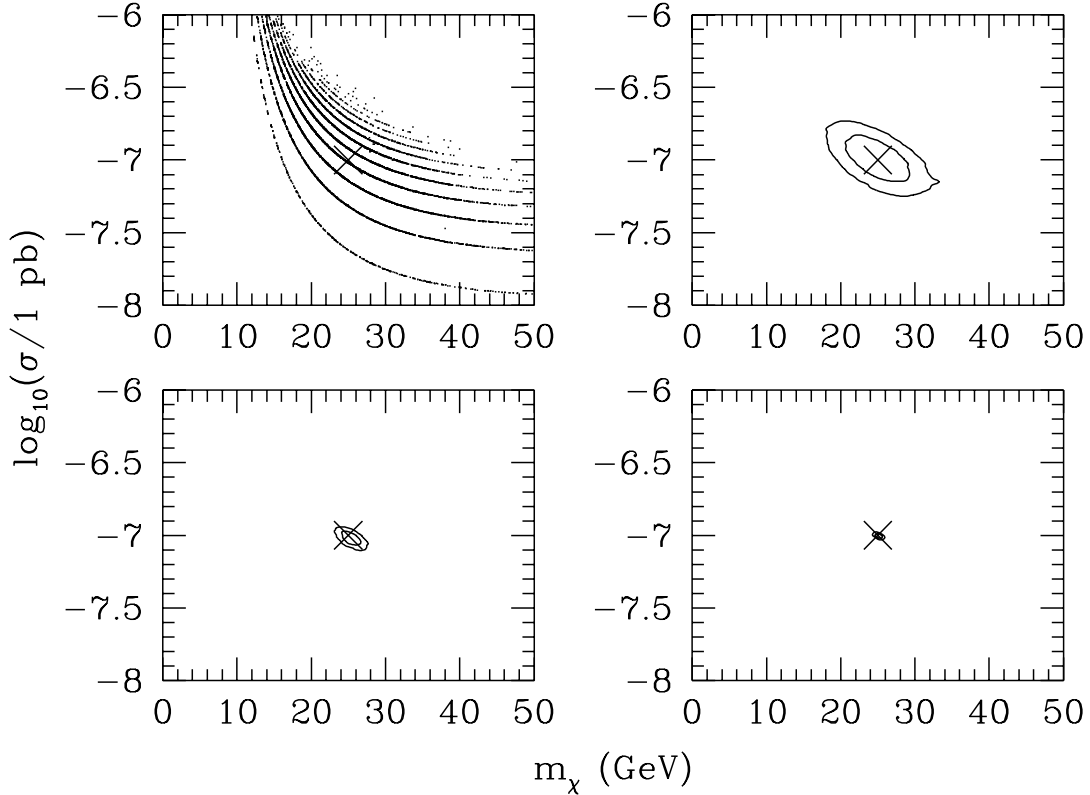


Figure 3. As fig. 2 for $m_\chi = 25$ GeV. For $\mathcal{E} = 3 \times 10^2$ kg day, $\lambda_{\text{in}} = 4.2$ and consequently there is a $\sim 1\%$ probability that an experiment would not detect any events.

them. The deviations of the kernel are chosen, for each exposure and underlying mass, to produce relatively smooth contours without artificially inflating the spread in the ML values. We then integrate the probability density above a threshold value and vary this threshold to find the values which enclose 68% and 95% of the probability distribution, and plot contours corresponding to these threshold values.

For the two smallest exposures there is a significant low probability density tail at large ML masses. This is due to the weak mass dependence of the characteristic energy E_R for $m_\chi > m_A$. For these exposures the majority of experiments have ML masses smaller than the input mass. The likelihood analysis is not biased, the expected value of the ML mass is equal to the input mass, however there are a significant number of experiments with ML masses substantially larger than the input mass. As the exposure is increased, λ_{in} becomes large and the fractional spread in the number of events observed in each experiment becomes small. This allows the interaction cross-section (which effectively acts as a normalization factor) to be accurately determined. The larger number of events also allows the energy dependence of the differential event rate, and hence the mass, to be determined more accurately.

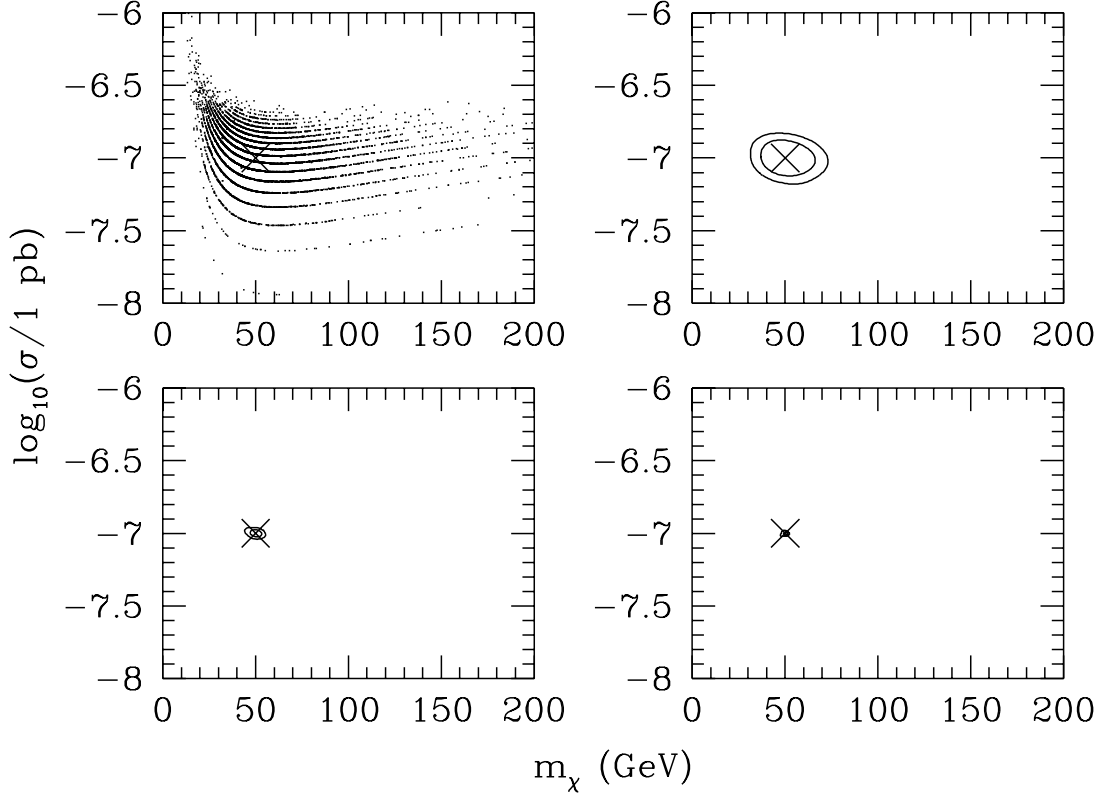


Figure 4. As fig. 2 for $m_\chi = 50$ GeV.

With an exposure of $\mathcal{E} = 3 \times 10^2$ kg day and an underlying WIMP mass of $m_\chi = 100$ GeV it will be difficult to make quantitative statements about the WIMP mass, beyond excluding very large or very small masses. Similarly it will not be possible to measure the cross-section more accurately than to within an order of magnitude. For $\mathcal{E} = 3 \times 10^3$ kg day the accuracy with which the mass can be determined improves, however there is still a significant tail of experiments finding ML masses substantially larger than the underlying value. More quantitatively 95% of experiments will find ML masses in the range $60 \text{ GeV} < m_\chi < 200 \text{ GeV}$. Increasing the exposure by an order of magnitude, the distribution of ML masses becomes more symmetric about the input mass and the spread in the ML masses is of order ± 30 GeV. With a further increase in the exposure to $\mathcal{E} = 3 \times 10^5$ kg day the mass could be measured to an accuracy of around 10 GeV (see the top panel of fig. 8 for a zoom in on the distribution in this case). The accuracy with which the cross-section can be measured increases with increasing exposure: $\Delta(\log \sigma_p) \sim \pm 0.2, 0.05$ and 0.02 for $\mathcal{E} = 3 \times 10^3, 3 \times 10^4$ and 3×10^5 kg day respectively. The shape of the distribution of ML parameters reflects the shape of curves of constant N_{expt} in the $m_\chi \sim 100$ GeV region, with a weak positive correlation between the best-fit values of m_χ and σ_p .

In figs. 3-6 we plot the results for input WIMP masses of $m_\chi = 25, 50, 250$ and

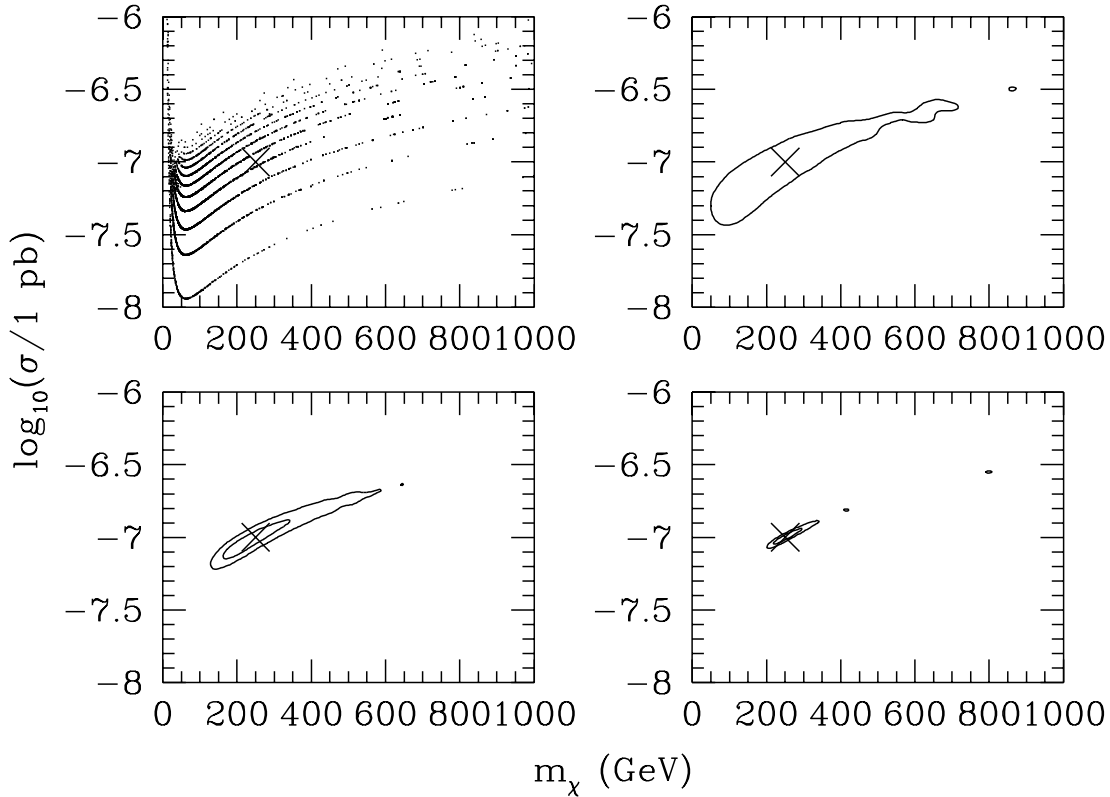


Figure 5. As fig. 2 for $m_\chi = 250$ GeV. For $\mathcal{E} = 3 \times 10^2$ kg day, $\lambda_{\text{in}} = 4.3$ and consequently there is a $\sim 1\%$ probability that an experiment would not detect any events. For $\mathcal{E} = 3 \times 10^3$ kg day there is a low probability density tail extending to large m_χ , and hence we can not accurately calculate a contour containing 95% of the probability density. The disconnected ‘blobs’ at large m_χ are also a consequence of this extended low probability density tail.

500 GeV respectively. For $m_\chi = 25, 250$ and 500 GeV the input mean number of events for $E = 3 \times 10^2$ kg day is small enough that there is a significant probability that an experiment will see no events (making it impossible to determine the WIMP mass).

For light WIMPs, $m_\chi < m_A$, the characteristic energy, E_R , varies significantly with WIMP mass. This allows the mass to be determined with large exposures more accurately than for $m_\chi = 100$ GeV. For an underlying mass of $m_\chi = 25$ GeV and an exposure of $\mathcal{E} = 2 \times 10^3$ kg day, due to the small expected number of events, it will be difficult to place meaningful constraints (beyond an upper limit on the mass) on the WIMP parameters. With larger exposures it will be possible to measure the WIMP mass and cross-section with increasing accuracy; for $\mathcal{E} = 3 \times 10^3, 3 \times 10^4$ and 3×10^5 kg day the distribution of ML WIMP masses is symmetric and 95% of experiments lie within $\pm 6, 4$ and 1 GeV of the input mass respectively. The accuracy with which σ_p can be measured improves roughly as for $m_\chi = 100$ GeV. For $m_\chi \sim 50$ GeV the fractional accuracy with which m_χ can be measured is similar; 95% of experiments lie within $\pm 12, 7, 2$ GeV of

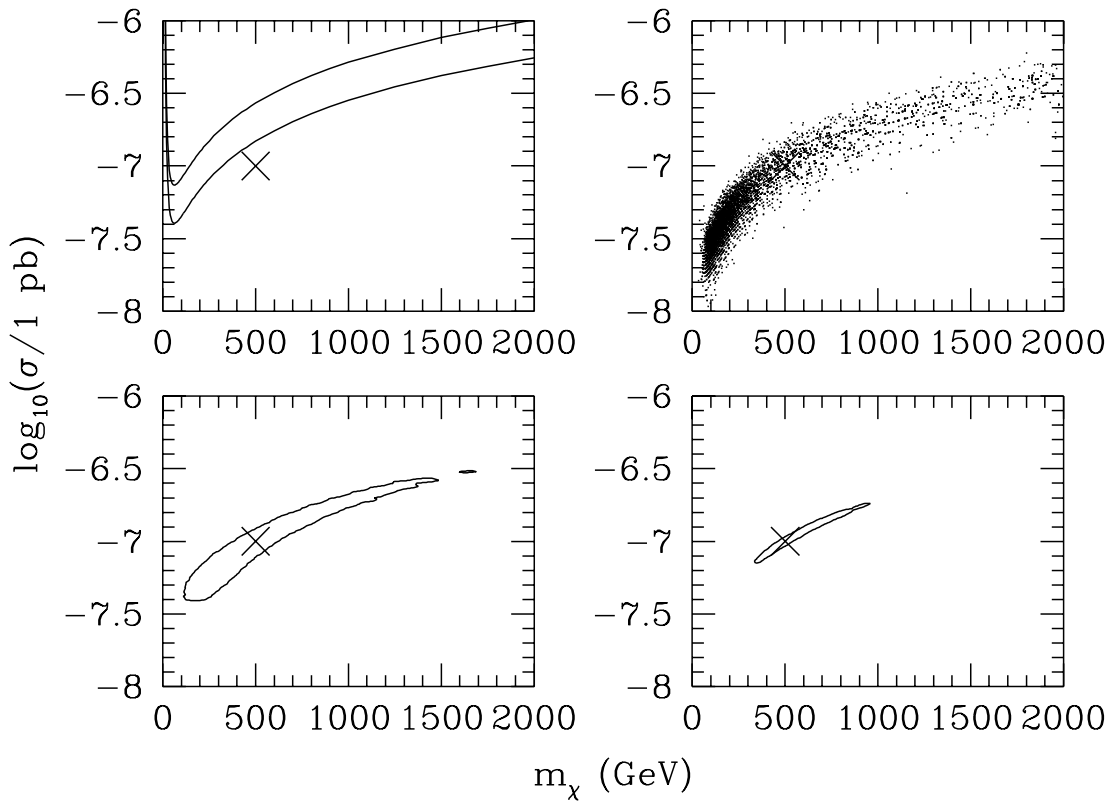


Figure 6. As fig. 2 for $m_\chi = 500$ GeV. For $\mathcal{E} = 3 \times 10^2$ kg day, $\lambda_{\text{in}} = 2.4$ and there is a $> 50\%$ probability that an experiment would observe two or fewer events. Consequently we instead plot the 68% and 95% exclusion limits which would be found by an experiment observing $N_{\text{exp}} = 2$ events (the number of observed events with the largest probability). For this input mass there is a low probability density tail extending to large m_χ , even for $\mathcal{E} = 3 \times 10^5$ kg day, and hence it is not possible to plot 95% probability contours.

the input mass for $\mathcal{E} = 3 \times 10^3$, 3×10^4 and 3×10^5 kg day respectively. The curves of constant N_{expt} are, for $m_\chi = 50$ GeV, roughly parallel to the m_χ axis, improving slightly the accuracy with which σ_p can be measured.

For massive WIMPs, $m_\chi \gg m_A$, the weak dependence of E_R on the WIMP mass means that there is a large spread in the distribution of ML masses even for large exposures. There is a small, but significant, probability that an experiment will happen to observe one or more unusually large energy events and hence find a large ($> \mathcal{O}(\text{TeV})$) ML mass. Because of the extremely weak dependence of the energy spectrum on the WIMP mass, the extended likelihood function also varies weakly with the mass in these cases (where the ML mass is of order a few TeV or greater, varying the WIMP mass by a factor of two from the ML value only changes the 4th significant figure of the log of the extended likelihood function). It is therefore not possible to determine the WIMP mass accurately in these cases.

For an underlying WIMP mass of $m_\chi = 250 \text{ GeV}$ and an exposure of $\mathcal{E} = 3 \times 10^2 \text{ kg day}$ it will be difficult to place any meaningful constraints on the WIMP parameters. As the exposure is increased it will be possible to place a lower limit on the mass: for $\mathcal{E} = 3 \times 10^3$, 3×10^4 and $3 \times 10^5 \text{ kg day}$, 95% of experiments have ML mass greater than 50, 125 and 200 GeV respectively. However it will not be possible to place an upper limit tighter than $m_\chi < \mathcal{O}(1 \text{ TeV})$ on the WIMP mass with a reasonable ($> 68\%$) degree of confidence. The shape of the curves of constant N_{exp} for $m_\chi \gg m_A$ mean that it will also be difficult to constrain σ_p . For $\mathcal{E} = 3 \times 10^4$ and $3 \times 10^5 \text{ kg}$, 95% of experiments lie within $\Delta(\log \sigma_p) \approx {}_{-0.2}^{+0.4}$ and ${}_{-0.1}^{+0.4}$ of the input value of σ_p (the asymmetric spread arises from the asymmetry in the distribution of ML masses).

The situation is even worse for an underlying WIMP mass of $m_\chi = 500 \text{ GeV}$. For $\mathcal{E} = 3 \times 10^2 \text{ kg day}$ there is a $> 50\%$ probability that an experiment will observe two or fewer events. In these circumstances rather than attempting to determine the WIMP mass and cross-section it would be more reasonable to instead determine the regions of WIMP mass-cross-section excluded. The observed number of events with the greatest probability is $N_{\text{exp}} = 2$. In the relevant panel of Fig. 6 we therefore plot the exclusion limits from the 68% and 95% upper limits on the underlying mean number of events if this number of events were observed, $\lambda < 3.5$ and 6.3 respectively. For $\mathcal{E} = 3 \times 10^4$ and $3 \times 10^5 \text{ kg day}$, 95% of experiments have ML mass greater than 125 and 350 GeV respectively, however it will not be possible to place an upper limit on the WIMP mass at more than 68% confidence. Similarly it will only be possible to place a lower limit on σ_p .

In fig. 7 we show the effect of the uncertainty in the value of the local circular speed, v_c , on the determination of m_χ . For an input WIMP mass of $m_\chi = 100 \text{ GeV}$ and an exposure of $\mathcal{E} = 3 \times 10^3 \text{ kg day}$ we vary v_c between 180 and 260 km s^{-1} [27]. The likelihood analysis is however carried out assuming $v_c = 220 \text{ km s}^{-1}$. We see in fig. 7 that there is a degeneracy between m_χ and v_c . The kinetic energies of the incoming WIMPs depend on their mass and velocities. For larger (smaller) v_c the incoming WIMPs have larger (smaller) mean kinetic energies than assumed, resulting in larger (smaller) ML mass values. This statement can be made more quantitative by differentiating the expression for the characteristic energy E_R , eq. (8):

$$\frac{\Delta m_\chi}{m_\chi} = -[1 + (m_\chi/m_A)] \frac{\Delta v_c}{v_c}. \quad (10)$$

This gives, for an input WIMP mass of $m_\chi = 100 \text{ GeV}$ a $\sim 20 \text{ GeV}$ shift in the WIMP mass from a 20 km s^{-1} uncertainty in v_c . However, as we see in fig. 7, the shape of the distribution of the ML parameters changes, in qualitatively the same way as when the underlying WIMP mass is changed. As v_c is decreased (increased) the expected number of events increases (decreases) and hence the best-fit cross-sections typically decrease (increase).

Finally in fig. 8 we examine the effect of the uncertainty in the detailed shape of the local velocity distribution. For an input WIMP mass of $m_\chi = 100 \text{ GeV}$ and the largest exposure, $\mathcal{E} = 3 \times 10^5 \text{ kg day}$, we use as input the logarithmic ellipsoidal model (which is

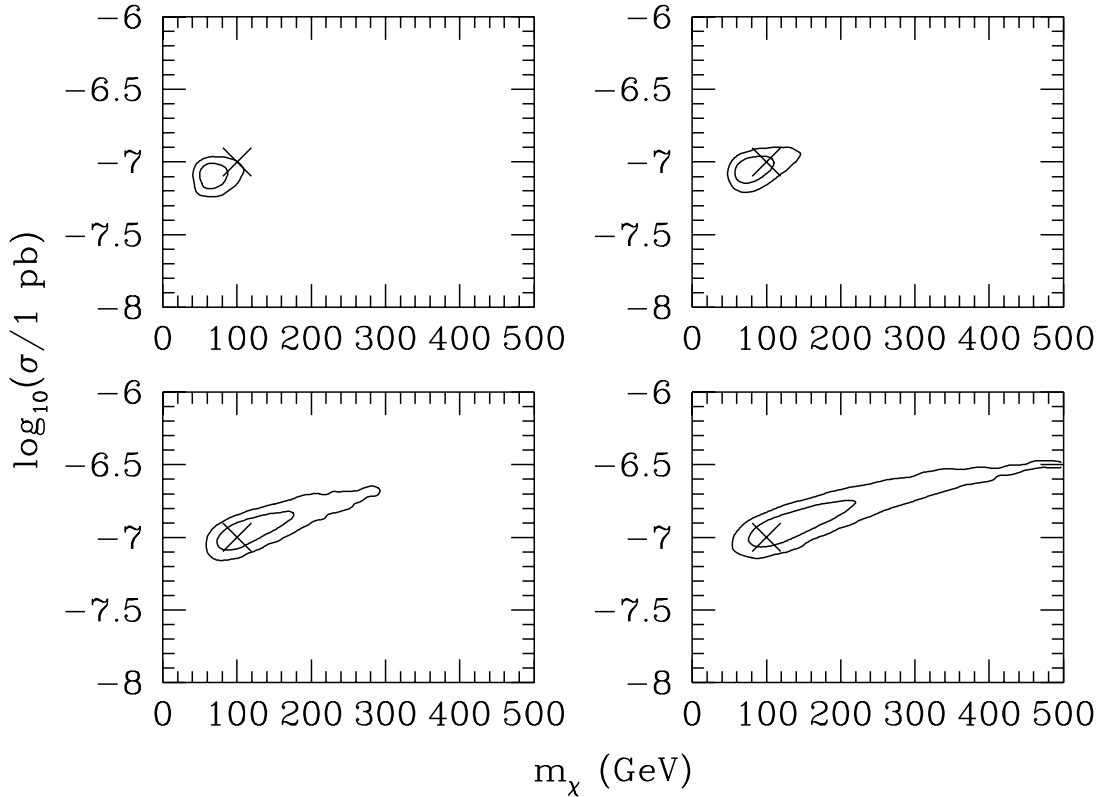


Figure 7. As fig. 2 but varying the input circular velocity $v_c = 180, 200, 240$ and 260 km s^{-1} with the exposure fixed at $\mathcal{E} = 3 \times 10^3 \text{ kg day}$. The maximum likelihood analysis is carried out assuming $v_c = 220 \text{ km s}^{-1}$.

the simplest triaxial generalization of the standard isothermal sphere) [30] and two of the sets of parameter values previously considered in Ref. [24]: $p = 0.9, q = 0.8, \gamma = 0.07$ and $p = 0.72, q = 0.7, \gamma = 4.0$ with the Earth located on the intermediate axis. These parameters correspond to axial ratios $1 : 0.78 : 0.48$ and $1 : 0.45 : 0.38$ (i.e. quite extreme triaxiality, especially in the second case) and, in both cases, velocity anisotropy $\beta = 0.1$. The local circular and escape speeds are kept fixed at the values used for the standard halo model. The likelihood analysis is carried out assuming the standard Maxwellian velocity distribution. Even for the second, quite extreme, model the shift in the typical ML mass from the underlying value is relatively small (less than 5 GeV). The small increase in the expected number of events for these halo models leads to a small downwards shift in the distribution of best-fit cross-sections.

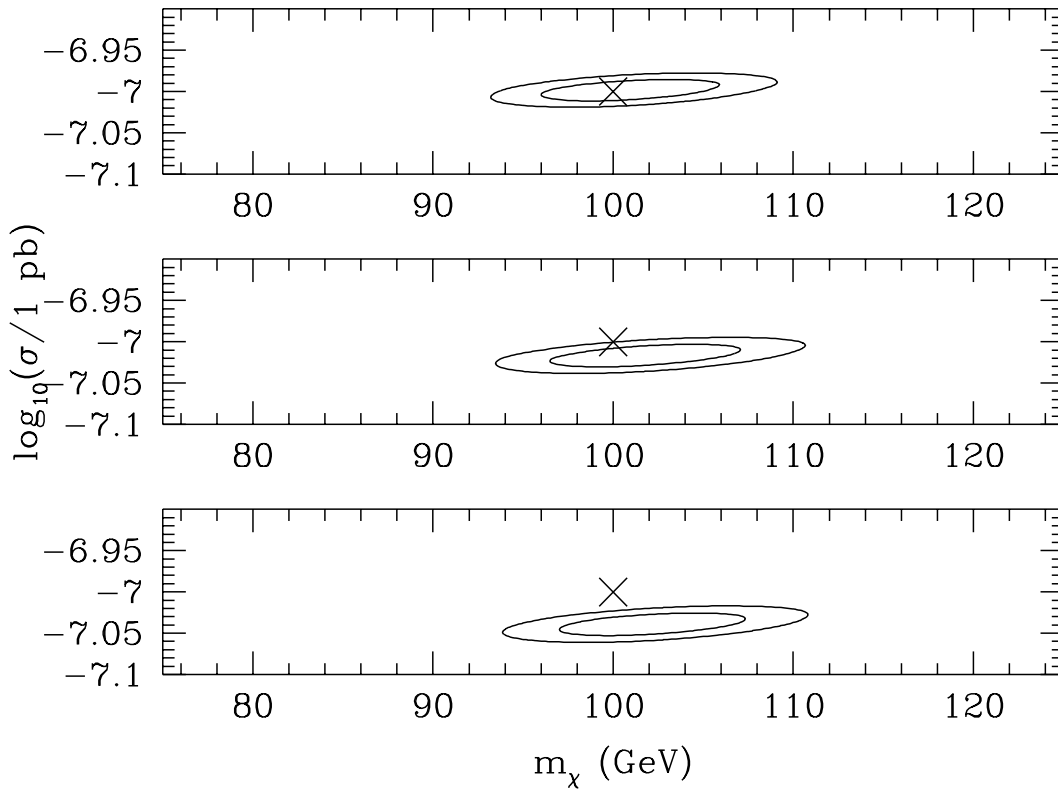


Figure 8. As fig. 7 but for the standard halo model (top panel) and the two non-standard halo models described in the text with the exposure fixed at $\mathcal{E} = 3 \times 10^5$ kg day. The maximum likelihood analysis is carried out assuming the standard Maxwellian speed distribution.

4. Validity of assumptions

4.1. WIMP distribution

Since the differential event rate is directly proportional to $\rho_\chi \sigma_p$, any uncertainty in the local WIMP density leads straightforwardly to an equivalent uncertainty in σ_p . We have fixed the local WIMP density to the ‘standard value’ of $\rho_\chi = 0.3 \text{ GeV cm}^{-3}$. Refs. [31, 32] found, using various observations to constrain the parameters of a range of halo models, local densities in the range $0.2 - 0.8 \text{ GeV cm}^{-3}$, which would lead to a factor of a few uncertainty in the determination of the cross-section.

We saw above that an uncertainty in the local circular velocity translates directly into an uncertainty in the measured WIMP mass. While the annual modulation signal depends sensitively on the WIMP velocity distribution [22], the *time averaged* differential event rates produced by smooth halo models are similar to that found under the standard assumption of a Maxwellian velocity distribution (e.g. [23, 24]). Hence, as we saw above, the uncertainty in the speed distribution, for fixed v_c , only leads to a small systematic

error in the determination of the WIMP mass (see fig. 8). In other words, for smooth halo models the characteristic energy of the energy spectrum, and hence the WIMP mass determination, depends only weakly on the detailed kinetic energy distribution. These smooth halo models are derived by solving the collisionless Boltzmann equation which assumes that the dark matter distribution has reached a steady state. The assumption that the local dark matter distribution is dynamically mixed, and hence smooth, is, however, a strong assumption, which may not be valid [33, 34]. Helmi, White & Springel [35] found that the 'particles' in a simulated Milky-Way like halo in a $\sim (\text{kpc})^3$ volume around the solar radius were relatively smoothly distributed. Direct detection experiments, however, probe the dark matter distribution on sub-milli-pc scales. The highest resolution simulations carried out to date have resolution of order $\mathcal{O}(100 \text{ pc})$ and hence can not resolve the dark matter distribution on the relevant scales.

In CDM cosmologies structure forms hierarchically and the local dark matter distribution will depend on the fate of the first, smallest, WIMP micro-halos to form. The mass of these microhalos is set by the WIMP microphysics in the early Universe [36], specifically kinetic decoupling and free-streaming, and (depending on the WIMP's interaction properties) is expected to lie in the range $10^{-12}M_\odot$ to $10^{-4}M_\odot$ [37]. The dynamical evolution of these micro-halos is being studied [38], however the detailed dark matter phase space distribution on sub-milli-pc scales is not yet known with any degree of certainty. If the local dark matter distribution consists of a small number of streams, with a-priori unknown velocities, then the energy spectrum would consist of a series of (sloping due to the energy dependence of the form factor) steps. The positions of these steps would depend on the WIMP mass and the (unknown) stream velocities, while the height of the steps would depend on the (unknown) stream density. In this case it would therefore not be possible to determine the WIMP mass from the energy spectrum.

4.2. Negligible background

From an experimental point of view, the most significant assumption is probably that of negligible background. Non-zero background could be incorporated (c.f. Ref. [39]) by simulating the recoil spectra produced by neutrons and including the background event rate (and additional parameters modeling the spectrum of the background events) in the maximum likelihood analysis. This would, however, require detailed modeling of the detector set-up and shielding. Adding additional parameters to the maximum likelihood analysis would clearly degrade the accuracy with which the WIMP mass and cross-section could be determined. The extent of the degradation would depend on the shape of the background energy spectrum (and how well it is known); the more similar it is to the WIMP spectrum the larger the errors will be.

4.3. Other sources of systematic error

Finite energy resolution and uncertainty in the form factor are other potential experimental sources of systematic error. The Helm form factor, with parameter values

as advocated by Lewin and Smith [7], deviates by only of order 1% from that calculated using electron elastic scattering data [40]. We have checked that Gaussian energy resolution, with full width at half maximum of order 1 keV [14], does not affect the WIMP parameters extracted from the energy spectrum ¶. Both of these issues are therefore likely to be less important than non-zero background and/or fine-grained structure in the WIMP distribution.

From a theoretical point of view the WIMP may have spin-dependent interactions⁺ with the nucleon and/or different coupling to the proton and neutron (e.g. Ref. [41, 42]). The measurement of the WIMP mass, in principle, in this case has been considered in Ref. [25].

5. Summary

We have examined the accuracy with which it will be possible to determine the WIMP mass from the energy spectrum observed in a SuperCDMS-like direct detection experiment given optimistic assumptions about the WIMP distribution and detector properties. If the WIMP distribution is smooth, the differential event rate varies with energy, modulo the energy dependence of the detector form factor, as $dR/dE \propto \exp(-E/E_R)$ where the characteristic energy, E_R , depends on the WIMP mass, m_χ . For light WIMPs ($m_\chi \ll m_A$ where m_A is the mass of the target nuclei) $E_R \propto m_\chi^2$, while for heavy WIMPs ($m_\chi \gg m_A$) $E_R \sim \text{const.}$ Consequently for light WIMPs the energy spectrum is strongly dependent on the WIMP mass, allowing the mass to be measured fairly accurately. For heavy WIMPs the dependence on the WIMP mass is far weaker making it difficult to measure the mass.

We have carried out Monte Carlo simulations of a SuperCDMS-like experiment composed of a Ge target with an energy threshold of 10 keV and zero background. We assumed, initially, that the local WIMP density is known and that the WIMP speed distribution is Maxwellian with local circular velocity $v_c = 220 \text{ km s}^{-1}$. For an optimistic interaction cross-section of $\sigma_p = 10^{-7} \text{ pb}$, just below the current exclusion limits from the CDMS experiment [12], we considered a range of WIMP masses, $25 \text{ GeV} < m_\chi < 500 \text{ GeV}$, and, efficiency weighted, exposures, $3 \times 10^2 \text{ kg day} < \mathcal{E} < 3 \times 10^5 \text{ kg day}$. For $\mathcal{E} = 3 \times 10^2 \text{ kg day}$ the expected number of events is small, the ML masses and cross-sections are stratified on curves of constant number of events and it would not be possible to obtain better than order of magnitude constraints on the WIMP parameters. For $\mathcal{E} = 3 \times 10^5 \text{ kg day}$ and an input mass of $m_\chi = 100 \text{ GeV}$ it would be possible, given the validity of the assumptions stated above, to measure the WIMP mass with accuracy $\pm 10 \text{ GeV}$ and the fractional cross-section with accuracy $\Delta(\log \sigma_p) = \pm 0.02$. The mass of lighter WIMPs could be measured more accurately, however for very light WIMPs,

¶ Since the underlying differential event rate is, modulo the form factor, close to exponential, Gaussian smoothing only changes its shape for energies of order the resolution (which are below the energy threshold).

⁺ Natural Germanium contains 7.7% ^{73}Ge which is sensitive to spin dependent interactions [42].

$m_\chi < \mathcal{O}(10 \text{ GeV})$, the number of events above the detector energy threshold would be too small to allow the mass to be measured accurately. For more massive WIMPs there is a significant tail of experiments with ML masses significantly larger than the input WIMP mass. For heavy WIMPs, $m_\chi > \mathcal{O}(500 \text{ GeV})$, even with $\mathcal{E} = 3 \times 10^5 \text{ kg day}$ it will only be possible to place lower limits on the WIMP mass and cross-section.

We then examined the effect of varying the underlying WIMP speed distribution for an input WIMP mass of 100 GeV . A change of $\pm 20 \text{ km s}^{-1}$ in the local circular speed, v_c , leads to a shift in the distribution of best fit WIMP mass of roughly $\pm 20 \text{ GeV}$ (although an increase in v_c leads, like an increase in the underlying WIMP mass, to a large tail of experiments with large best fit masses). Changing the shape of the WIMP velocity distribution, while keeping v_c fixed, leads to only a small change in the input energy spectrum and hence the shift in the best fit WIMP masses is relatively small, $< \mathcal{O}(5 \text{ GeV})$, even for quite extreme smooth halo models. There is, for smooth halo models, a factor of a few uncertainty in the local WIMP density [31, 32] which leads to a corresponding uncertainty in σ_p . The assumption of a smooth WIMP distribution may well, however, not be valid. The local WIMP distribution, on sub milli-pc scales, may be composed of a (a priori unknown) number of discrete streams with unknown velocities. If this is the case it will not be possible to extract constraints on the WIMP mass from an observed signal.

Finally we discussed the validity of the other assumptions made, namely negligible background, purely spin independent coupling, perfect energy resolution and known detector form factor. Of these negligible background is probably the most significant and could in principle be taken into account by simulating the recoil spectra produced by neutrons and including the background event rate and energy spectrum in the maximum likelihood analysis.

Acknowledgments

AMG is supported by PPARC and is grateful to Ben Morgan and Simon Goodwin for useful discussions and Meghan Gray and Chris Conselice for assistance with supermongo contour plotting.

6. References

- [1] M. Tegmark et al., Phys. Rev. D **69** 103501 (2004), [astro-ph/0310723](#); D. J. Eisenstein et al., Astrophys. J **633**, 560 (2005), [astro-ph/0501171](#); S. Cole et al., Mon. Not. Roy. Astron. Soc. **362**, 505 (2005), [astro-ph/0501174](#); D. N. Spergel et al., [astro-ph/0603449](#).
- [2] G. Jungman, M. Kamionkowski and K. Griest, Phys. Rep. **267**, 195 (1996).
- [3] L. Bergström, Rept. Prog. Phys. **63**, 793 (2000), [hep-ph/0002126](#); G. Bertone, D. Hooper and J. Silk, Phys. Rep. **405** 279 (2005), [hep-ph/0404175](#).
- [4] M. W. Goodman and E. Witten, Phys. Rev. D **31**, 3059 (1985).
- [5] E. A. Baltz, M. Battaglia, M. E. Peskin and T. Wizansky, Phys. Rev. D **74** 103521 (2006), [hep-ph/0602187](#).

- [6] D. Hooper and A. M. Taylor, [hep-ph/0607086](#); M. Carena, D. Hooper and A. Vallinoto, [hep-ph/0611065](#).
- [7] J. D. Lewin and P. F. Smith, *Astropart. Phys.* **6**, 87 (1996).
- [8] A. K. Drukier, K. Freese and D. N. Spergel, *Phys. Rev. D* **33**, 3495 (1986); K. Freese, J. Frieman and A. Gould, *Phys. Rev. D* **37**, 3388 (1988).
- [9] J. R. Primack, D. Seckel and B. Sadoulet, *Ann. Rev. Nucl. Part. Sci.* **38**, 751 (1988).
- [10] F. Hasenbalg, *Astropart. Phys.* **9**, 339 (1998), [astro-ph/9806198](#).
- [11] M. J. Lewis and K. Freese, *Phys. Rev. D* **70** 043501 (2004), [astro-ph/0307190](#).
- [12] D. S. Akerib et al., *Phys. Rev. Lett.* **96** 011302 (2006), [astro-ph/0509269](#).
- [13] D. S. Akerib et al., *Phys. Rev. D* **72**, 052009 (2005), [astro-ph/0507190](#).
- [14] R. W. Schnee et al., proceedings of DARK 2004, fifth international Heidelberg conference on dark matter in Astro and Particle Physics, [astro-ph/0502435](#).
- [15] P. L. Brink et al., proceedings of Texas Symposium on Relativistic Astrophysics (2004), [astro-ph/0503583](#).
- [16] E. Aprile et al., [astro-ph/0502279](#).
- [17] H. Kraus et al., *J. Phys. Conf. Ser.* **39** 139 (2006).
- [18] Y. Ramachers, *Astroparticle Physics* **19**, 419 (2003).
- [19] R. Bernabei et al., *Phys. Lett.* **B389**, 757 (1996); *ibid* **B408**, 439 (1997); *ibid* **B424**, 195 (1998); *ibid* **B450**, 448 (1999); *ibid* **B480**, 23 (2000). R. Bernabei et al., *Riv. Nuovo. Cim.* **26N1** 1 (2003), [astro-ph/0307403](#).
- [20] A. Kurylov and M. Kamionkowski, *Phys. Rev. D* **69**, 063503 (2004), [hep-ph/037185](#).
- [21] D. Smith and N. Weiner, *Phys. Rev. D* **64**, 043502 (2001) [hep-ph/0101138](#); D. Tucker-Smith and N. Weiner, *Phys. Rev. D* **72**, 063520, (2005) [hep-ph/0402065](#).
- [22] J. D. Vergados, *Phys. Rev. Lett.* **83**, 3597 (1999); P. Belli et. al., *Phys. Rev. D* **61**, 023512 (2000) [hep-ph/9903501](#); J. D. Vergados, *Phys. Rev. D* **62**, 023519 (2000) [astro-ph/0001190](#); *Phys. Rev. D* **63** 063511 (2001) [hep-ph/0101019](#); A. M. Green, *Phys. Rev. D* **63**, 043005 (2001) [astro-ph/0008318](#); *Phys. Rev. D* **63** 103003 (2001) [astro-ph/0012393](#); G. Gelmini and P. Gondolo, *Phys. Rev. D* **64**, 023504 (2001); P. Belli, R. Cerulli, N. Forengo and S. Scopel, *Phys. Rev. D* **66**, 043503 (2002) [hep-ph/0203242](#); J. D. Vergados and D. Owen, *Astrophys. J.* **589**, 17 (2003) [astro-ph/0203293](#); C. J. Copi and L. M. Krauss, *Phys. Rev. D* **67** 103507 (2003) [astro-ph/0208010](#); N. Fornengo and S. Scopel, *Phys. Lett. B* **576** 189 (2003) [astro-ph/0301132](#); J. D. Vergados, *Phys. Rev. D* **67** 103003 (2003) [astro-ph/0303231](#) A. M. Green, *Phys. Rev. D* **68**, 023004 (2001) [astro-ph/0304446](#).
- [23] M. Kamionkowski and A. Kinkhabwala, *Phys. Rev. D* **57**, 3256 (1998), [hep-ph/9710337](#); F. Donato, N. Fornengo and S. Scopel, *Astropart. Phys.* **9**, 247 (1998), [hep-ph/9803295](#).
- [24] A. M. Green, *Phys. Rev. D* **66**, 083003 (2002), [astro-ph/0207366](#).
- [25] J. L. Bourjaily and G. L. Kane, [hep-ph/0501262](#).
- [26] R. H. Helm, *Phys. Rev.* **104** 1466 (1956).
- [27] F. J. Kerr and D. Lynden-Bell, *Mon. Not. Roy. Astron. Soc.* **221**, 1023 (1986).
- [28] M. C. Smith et al., [astro-ph/0611671](#).
- [29] G. Cowan, *Statistical data analysis*, published by Oxford University Press (1998).
- [30] N. W. Evans, C. M. Carollo and P. T. de Zeeuw, *Mon. Not. Roy. Astron. Soc.* **318**, 1131 (2000), [astro-ph/0008156](#).
- [31] E. I. Gates, G. Gyuk and M. S. Turner, *Astrophys. J.* **449**, L123 (1995), [astro-ph/9505039](#).
- [32] L. Berström, P. Ullio and J. H. Buckley, *Astropart. Phys.* **9** 137 (1998), [astro-ph/9712318](#).
- [33] B. Moore et al., *Phys. Rev. D* **64** 063508 (2001), [astro-ph/0106271](#).
- [34] S. Stiff and L. Widrow, *Phys. Rev. Lett.* **90**, 211301 (2003), [astro-ph/0301301](#).
- [35] A. Helmi, S. D. M. White and V. Springel, *Phys. Rev. D* **66**, 0635023 (2002), [astro-ph/0201289](#).
- [36] S. Hofmann, D. Schwarz and H. Stöcker, *Phys. Rev. D* **64** 083507 (2001), [astro-ph/0104173](#); V. Berezhinsky, V. Dokuchaev and Y. Eroshenko, *Phys. Rev. D* **68** 103003 (2003), [astro-ph/0301551](#); A. M. Green, S. Hofmann and D. J. Schwarz, *Mon. Not. Roy. Astron.*

- Soc. **353**, L23 (2004), [astro-ph/0309621](#); JCAP 0508 (2005) 003, [astro-ph/0508553](#); A. Loeb and M. Zaldarriaga, Phys. Rev. D **71** 103520 (2005), [astro-ph/0504112](#); E. Bertschinger, Phys. Rev. D **74** 063509 (2006), [astro-ph/0607319](#).
- [37] S. Profumo, K. Sigurdson and M. Kamionkowski, Phys. Rev. Lett. **97** 031301 (2006), [astro-ph/0603373](#).
- [38] J. Diemand, B. Moore and J. Stadel, Nature **433**, 389 (2005), [astro-ph/0501589](#); V. Berezhinsky, V. Dokuchaev and Y. Eroshenko, Phys. Rev. D **73** 063504 (2006), [astro-ph/0511494](#); H. Zhao, D. Hooper, G. W. Angus, J. E. Taylor and J. Silk, Astrophys. J **654**, 697 (2007), [astro-ph/0508215](#); A. M. Green and S. P. Goodwin, Mon. Not. Roy. Astron. Soc. **375**, 1111 (2007), [astro-ph/0604142](#); T. Goerdt, O. Y. Gnedin, M. Moore, J. Diemand and J. Stadel, Mon. Not. Roy. Astron. Soc. **375**, 191 (2007), [astro-ph/0608495](#); G. W. Angus and H. Zhao Mon. Not. Roy. Astron. Soc. **375**, 1146 (2007), [astro-ph/0608580](#).
- [39] H. Kraus et al., Phys. Lett. B **610** 37 (2005).
- [40] G. Duda, A. Kemper and P. Gondolo, [hep-ph/0608035](#).
- [41] P. Ullio, M. Kamionkowski and P. Vogel, J. High Energy Phys. **07**:044 (2001), [hep-ph/0010036](#); A. Kurylov and M. Kamionkowski, Phys. Rev. D **69**, 063503 (2004), [hep-ph/0307185](#); F. Giuliana, Phys. Rev. Lett. **93**, 161301 (2004), [hep-ph/0405215](#); C. Savage, P. Gondolo and K. Freese, Phys. Rev. D **70**, 123513 (2004), [astro-ph/0408346](#).
- [42] D. S. Akerib et al., Phys. Rev. D **73**, 011102 (2006), [astro-ph/0509269](#).